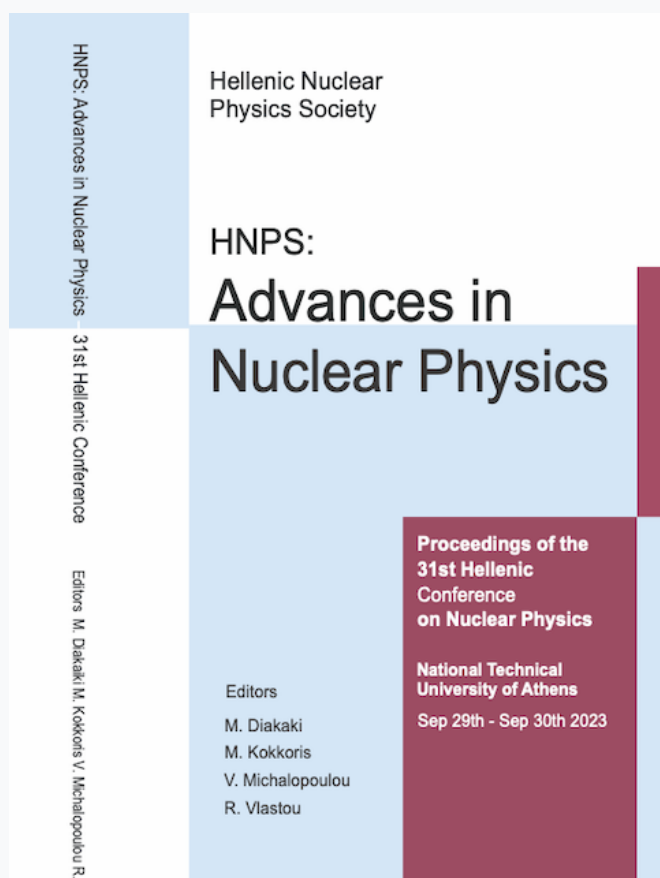


# HNPS Advances in Nuclear Physics

Vol 30 (2024)

HNPS2023



## Lifetime measurement in $^{182}\text{W}$ using the Differential Decay Curve Method

*Aikaterini Zyriliou, Theodoros Mertzimekis, Polytimos Vasileiou, Eirini Mavrommatis, Achment Chalil, Margarita Efstathiou, Angelos Karadimas, Dennis Bonatsos, Andriana Martinou, Nikolay Minkov, Nicolae Marginean, Constantin Mihai, Nicoleta Florea, Ruxandra Borcea, Sorin Ujenuc, Andrei Turturica, Cristian Costache, Radu Mihai, Lucian Stan, Dan Filipescu, Sebastian Toma, Ioana Gheorghe, Irina Dinescu, Alina Ionescu, Liviu Stoica, Stefana Calinescu, Andreea Oprea, Alexandru Stoica, Christophe Sotty, Cristina Clisu, Cristina Nita, Catalin Neacsu, Marian Boromiza, Radu Marginean, Dorel Bucurescu, Razvan Lica, Lucian Stroe, Rares Suvaila*

doi: [10.12681/hnpsanp.6283](https://doi.org/10.12681/hnpsanp.6283)

Copyright © 2024, Aikaterini Zyriliou, Theodoros Mertzimekis, Polytimos Vasileiou, Eirini Mavrommatis, Achment Chalil, Margarita Efstathiou, Angelos Karadimas, Dennis Bonatsos, Andriana Martinou, Nikolay Minkov, Nicolae Marginean, Constantin Mihai, Nicoleta Florea, Ruxandra Borcea, Sorin Ujenuc, Andrei Turturica, Cristian Costache, Radu Mihai, Lucian Stan, Dan Filipescu, Sebastian Toma, Ioana Gheorghe, Irina Dinescu, Alina Ionescu, Liviu Stoica, Stefana Calinescu, Andreea Oprea, Alexandru Stoica, Christophe Sotty, Cristina Clisu, Cristina Nita, Catalin Neacsu, Marian Boromiza, Radu Marginean, Dorel Bucurescu, Razvan Lica, Lucian Stroe, Rares Suvaila



This work is licensed under a [Creative Commons Attribution-NonCommercial-NoDerivatives 4.0](https://creativecommons.org/licenses/by-nc-nd/4.0/).

**To cite this article:**

Zyriliou, A., Mertzimekis, T., Vasileiou, P., Mavrommatis, E., Chalil, A., Efstathiou, M., Karadimas, A., Bonatsos, D., Martinou, A., Minkov, N., Marginean, N., Mihai, C., Florea, N., Borcea, R., Ujeniuc, S., Turturica, A., Costache, C., Mihai, R., Stan, L., Filipescu, D., Toma, S., Gheorghe, I., Dinescu, I., Ionescu, A., Stoica, L., Calinescu, S., Oprea, A., Stoica, A., Sotty, C., Clisu, C., Nita, C., Neacsu, C., Boromiza, M., Marginean, R., Bucurescu, D., Lica, R., Stroe, L., & Suvaila, R. (2024). Lifetime measurement in  $^{182}\text{W}$  using the Differential Decay Curve Method. *HNPS Advances in Nuclear Physics*, *30*, 43–50. <https://doi.org/10.12681/hnpsanp.6283>

## Lifetime measurement in $^{182}\text{W}$ using the Differential Decay Curve Method

A. Zyriliou<sup>1,\*</sup>, T.J. Mertzimekis<sup>1</sup>, P. Vasileiou<sup>1</sup>, E. Mavrommatis<sup>1</sup>, A. Chalil<sup>1,2</sup>, M. Efstathiou<sup>1</sup>,  
A. Karadimas<sup>1</sup>, D. Bonatsos<sup>3</sup>, A. Martinou<sup>3</sup>, N. Minkov<sup>4</sup>, N. Marginean<sup>5</sup>, C. Mihaï<sup>5</sup>,  
N. Florea<sup>5</sup>, R. Borcea<sup>5</sup>, S. Ujenuc<sup>5</sup>, A. Turturica<sup>5</sup>, C. Costache<sup>5</sup>, R. Mihaï<sup>5</sup>, L. Stan<sup>5</sup>,  
D. Filipescu<sup>5</sup>, S. Toma<sup>5</sup>, I. Gheorghe<sup>5</sup>, I. Dinescu<sup>5</sup>, A. Ionescu<sup>5</sup>, L. Stoica<sup>5</sup>, S. Calinescu<sup>5</sup>,  
A. Oprea<sup>5</sup>, A. Stoica<sup>5</sup>, C. Sotty<sup>5</sup>, C. Clisu<sup>5</sup>, C. Nita<sup>5</sup>, C. Neascu<sup>5</sup>, M. Boromiza<sup>5</sup>,  
R. Marginean<sup>5</sup>, D. Bucurescu<sup>5</sup>, R. Lica<sup>5</sup>, L. Stroe<sup>5</sup>, R. Suvaila<sup>5</sup>

<sup>1</sup> Department of Physics, National and Kapodistrian University of Athens, Greece

<sup>2</sup> Université Claude Bernard Lyon 1, CNRS/IN2P3, IP2I Lyon, Villeurbanne, France

<sup>3</sup> Institute of Nuclear and Particle Physics, NCSR “Demokritos”, Greece

<sup>4</sup> Institute of Nuclear Research and Nuclear Energy, Bulgarian Academy of Sciences, Bulgaria

<sup>5</sup> Horia Hulubei National Institute of Physics and Nuclear Engineering, Romania

**Abstract** This work focuses on the lifetime measurement and spectroscopic properties of  $^{182}\text{W}$ . The mass region around this nucleus is of significant interest due to its unexplored nature and the presence of intriguing structural phenomena, including deformation, shape changes, and shape coexistence. Experimental measurements were conducted in the National Laboratory IFIN-HH in Romania, focused on the spectroscopic study of  $^{182}\text{W}$  isotope using the Differential Decay Curve Method (DDCM), a similar approach for the Recoil Distance Doppler Shift (RDDS) method. This experiment provided valuable data on the energy levels, lifetimes, and decay properties of the excited states in the  $^{182}\text{W}$  and neighboring nuclei. The measurements were performed using the ROSPHERE detector array, loaded with HPGe and particle identification detectors, and a plunger device. As a result, the lifetime for the  $6_1^+$  in  $^{182}\text{W}$  obtained for the first time via the fusion evaporation reaction  $^{181}\text{Ta}(^{11}\text{B}, ^{10}\text{Be})^{182}\text{W}$  and the DDCM at 47 MeV, and was found to agree well with earlier measurements.

**Keywords** lifetime, RDDS, DDCM, fusion evaporation reaction

## INTRODUCTION

The heavy mass region around  $A \sim 180$  displays interesting nuclear structural phenomena, marked by transitions between prolate and oblate shapes and the emergence of triaxial deformation from deformed mass distributions. This makes the transitional  $^{172-186}\text{W}$  nuclei in this heavy neutron-rich mass range particularly intriguing for studying the interplay between triaxial and axially deformed nuclear shapes [1]. Moreover, these tungsten isotopes serve as a crucial link connecting the deformed rare-earth region with the spherical nuclei near  $Z=82$ , exhibiting stable triaxial shapes in their ground states [2]. Additionally, a maximum in  $\gamma$ -softness is predicted at  $N=116$  for the W and Os isotopic chains [3].

The shape of a nucleus is significantly influenced by the  $R_{4/2} = E(4_1^+)/E(2_1^+)$  ratio, a key indicator of rotor behavior. A spherical nucleus typically has an  $R_{4/2}$  value around 2, a non-axial gamma-soft rotor hovers at 2.5, and a symmetric rigid rotor approaches 3.33. In this investigation, the W isotopes exhibit  $R_{4/2}$  values near the limit of a symmetric rigid rotor. For instance,  $^{182}\text{W}$  (Fig. 1) reaches the maximum value of 3.29, gradually decreasing to a minimum of 2.73 for  $^{190}\text{W}$ . The lighter isotope,  $^{172}\text{W}$ , has a ratio greater than 3 ( $R_{4/2} = 3.06$ ). The behavior of  $R_{4/2}$  confirms that  $^{182}\text{W}$  is the most deformed isotope among those examined, a characteristic further supported by the maxima of the  $R_{2/1} = E(2_2^+)/E(2_1^+)$  ratio, as detailed in Table 2 of the referenced publication [1]. Here,  $E(2_2^+)$  signifies the excitation energy of the

\* Corresponding author: [kzyriliou@phys.uoa.gr](mailto:kzyriliou@phys.uoa.gr)

$\gamma$ -vibration band head, while  $E(2_1^+)$  represents the energy of the first excited state. Both  $R_{4/2}$  and  $R_{2/1}$  ratios decrease for  $N > 108$ , signifying an increase in  $\gamma$ -softness.

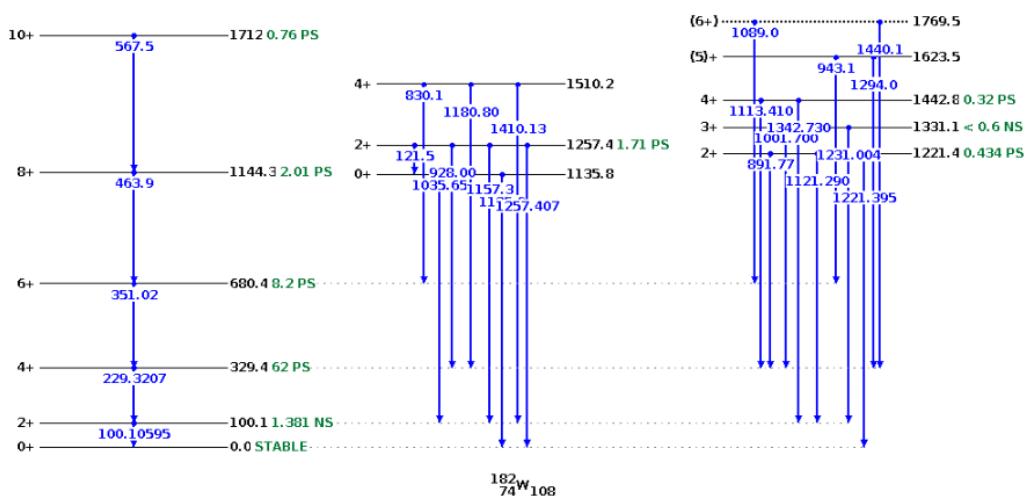


Figure 1. Partial level scheme of  $^{182}\text{W}$  isotope showing g.s.,  $\beta$  and  $\gamma$  bands [4]

## EXPERIMENTAL DETAILS

A beam of  $^{11}\text{B}$  was accelerated at 47 MeV using the 9 MV Tandem accelerator at the IFIN-HH laboratory in Magurele, Romania. This beam was directed onto a  $1\text{ mg/cm}^2$  self-supported metallic  $^{nat}\text{Ta}$  target, composed of 99.99% natural abundance of  $^{181}\text{Ta}$  (see Fig. 2). The aim was to populate the excited states in  $^{182}\text{W}$  through the stripping reaction  $^{181}\text{Ta}(^{11}\text{B},^{10}\text{Be})^{182}\text{W}$ . The detection of the  $\gamma$  rays from product nuclei was carried out using the ROSPHERE array [5], in its configuration of 25 HPGe detectors (see Fig. 3). The SORCERER solar cell particle detector array [6] was coupled to ROSPHERE, enabling the implementation of particle- $\gamma$  and particle- $\gamma$ - $\gamma$  coincidence techniques to selectively identify the decays of interest.

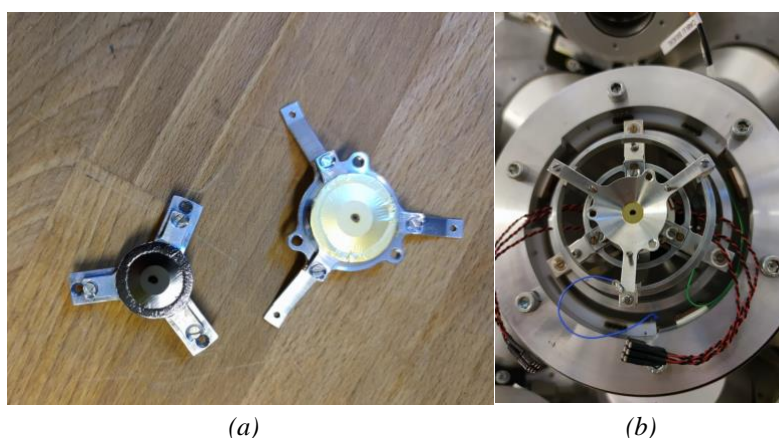
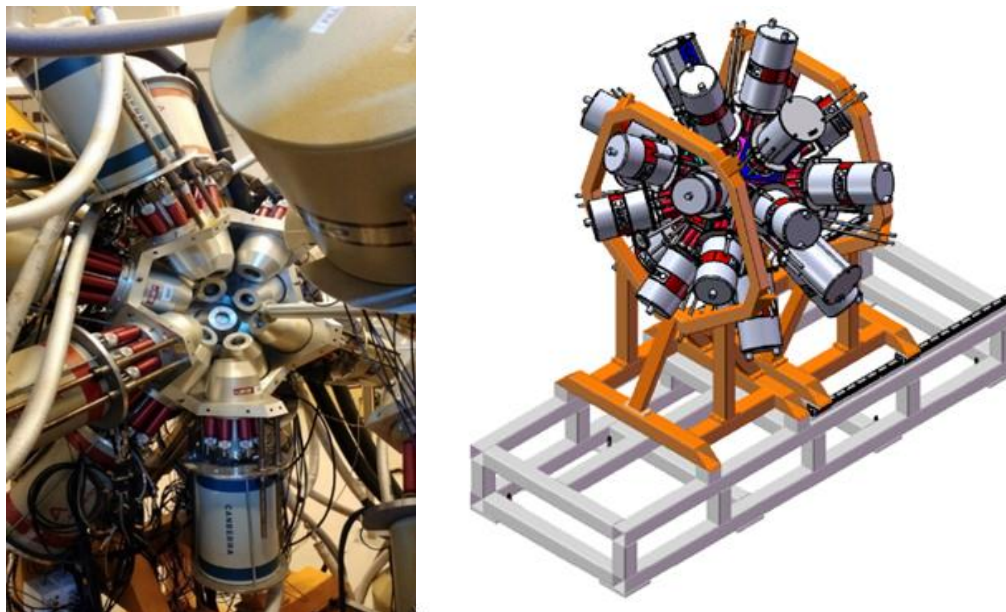


Figure 2. (a) Ta target (left) and Au stopper (right) for the plunger device and (b) the Au stopper mounted in the plunger device

For the measurement of lifetimes of excited states in  $^{182}\text{W}$ , the Differential Decay Curve Method (DDCM) was employed [7]. This technique mandates a device capable of achieving and consistently maintaining a micrometer ( $\mu\text{m}$ ) range distance between the target and stopper foils. Commonly referred to as a “plunger device” in literature due to its shape, this device plays a critical role in ensuring precise distances are maintained throughout the measurement process. In our experiment, a plunger device with

a  $^{197}\text{Au}$  stopper of  $3\text{ mg/cm}^2$  thickness (Fig. 2) was utilized at six different distances, ranging from 15 to 260  $\mu\text{m}$ . The configuration of the detector array used in our experiment is depicted in Fig. 3.



**Figure 3.** View of the ROSPHERE array with 25 HPGe detectors

### Experimental Technique

The Differential Decay Curve Method (DDCM), which was employed in this study, is an experimental technique designed for the measurement of lifetimes of excited nuclear states within the range of  $10^{-12}$  to  $10^{-8}$  s [8-9]. This method takes advantage of the Doppler effect, which affects the emitted  $\gamma$  rays while the recoil is in-flight, as also does the Recoil Distance Doppler Shift (RDDS) method [10]. In the latter, the level of interest is excited at time  $t=0$  through a beam-induced nuclear reaction in a thin target. Following the momentum transferred to the excited nucleus during the reaction, it exits the target with a velocity  $u$  and at an angle  $\theta$  relative to the beam direction. Subsequently, it comes to rest after a well-defined flight time  $t_f=x/u$  in a stopper foil, where  $x$  represents the separation distance between the target and the stopper. This arrangement is schematically depicted in Fig. 4a.

The lifetimes of the excited nuclear states are determined by analyzing the dependence of the intensity ratio between the shifted and unshifted components of the transition of interest on the distance separating the target and the stopper. Depending on the distance, some nuclei may not reach the stopper foil before decaying, and consequently, they decay in flight, emitting  $\gamma$  rays that are Doppler-shifted. By comparing the changes in the areas of the shifted and unshifted peaks for varying target-stopper distances, the lifetime of interest can be accurately determined.

Within the DDCM analysis framework [11], it becomes feasible to determine a lifetime for each target-to-stopper distance. To determine the lifetime of a nuclear state, it is essential to measure at least three target-stopper distances within the sensitive region [12].

In DDCM  $\gamma$ - $\gamma$  coincidence analysis, two common conditioning techniques are used: *direct* and *indirect*. In direct conditioning, a gate is applied to the shifted component of the transition that directly feeds the level of interest. This implies that only gamma rays emitted during the in-flight decay of the directly feeding transition are selected and analyzed. On the other hand, in indirect conditioning, a gate is applied to the shifted component of the transition that indirectly feeds the level of interest through an intermediary level. This means that only gamma rays emitted during the in-flight decay of the indirectly feeding transition, subsequently populating the level of interest, are selected and analyzed.

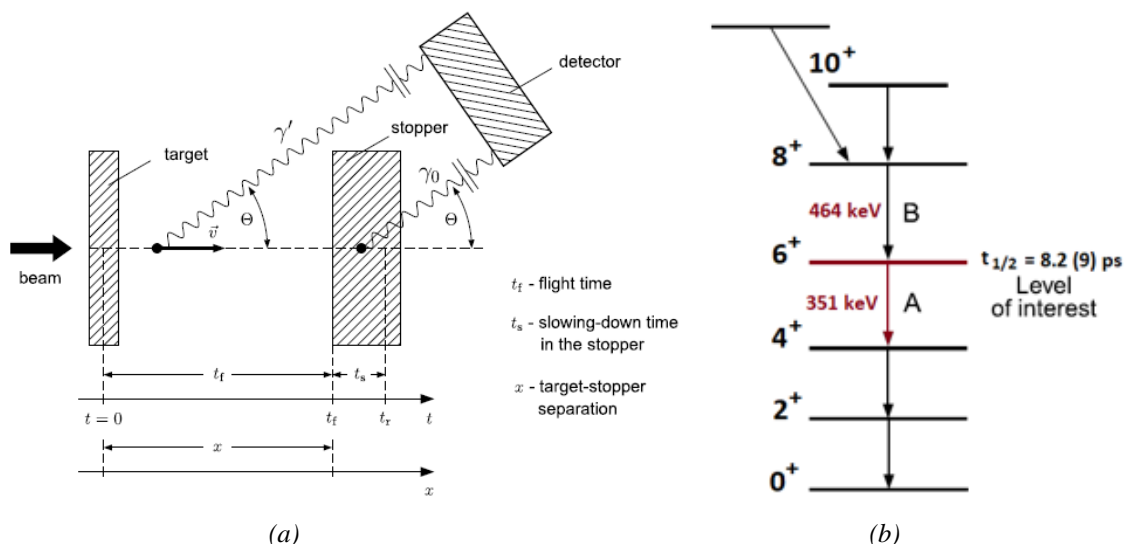


**Figure 4.** (a) A schematic description of the Recoil Distance Doppler Shift method [7]. (b) Selected cascade with feeding only via B by gating in the shifted component of B for  $^{182}\text{W}$  isotope ( $8^+ \rightarrow 6^+$  at 464 keV).

Both direct and indirect conditioning techniques are valuable in DDCM  $\gamma$ - $\gamma$  coincidence analysis, allowing for the isolation and study of specific decay pathways and their associated lifetimes. The choice between direct and indirect conditioning depends on the specific experimental setup and the decay scheme of the nuclear states under investigation. In the direct conditioning used in this study (see Fig. 4b), the lifetime of the state of interest can be determined using Eq. (1) [10]:

$$\tau(x) = \frac{I_{u_A}^{SB}(x)}{\frac{d}{dx} I_{s_A}^{SB}(x)} \frac{1}{u} \quad (1)$$

The intensities of the unshifted  $I_{u_A}^{SB}(x)$  and the shifted  $I_{s_A}^{SB}(x)$  components of the A transition are experimentally measured for each target to stopper distance. The derivative which fits the Doppler shifted intensities  $I_{s_A}^{SB}(x)$  is estimated by region fitting using second degree polynomials which are continuous and differentiable.

## RESULTS AND DISCUSSION

To begin the spectroscopic analysis, it is important to exclude other isotopes and concentrate solely on the nucleus of interest. Along with  $^{182}\text{W}$ , various isotopes in this region were produced through different reaction channels, as illustrated in Fig. 5, with lighter particles being identified by Si detectors. This study is exclusively focused on the highlighted area, where the ejectile  $^{10}\text{Be}$  coincides with the  $^{182}\text{W}$  nucleus, accomplished by implementing a coincidence condition (gate) in these channels.

In Fig. 6, the  $\gamma$ - $\gamma$  spectrum is presented at 47 MeV beam energy and 150  $\mu\text{m}$  target to stopper distance. Several transitions in the ground state band and side bands of  $^{182}\text{W}$  isotopes are observed. Also, due to the interaction of  $^{197}\text{Au}$  stopper with the  $^{11}\text{B}$  beam, transitions from  $^{198}\text{Hg}$  were detected. The contributions from the Coulex of  $^{181}\text{Ta}$  (target) and  $^{197}\text{Au}$  (stopper) are significantly smaller. The same procedure was followed for the other distances, as well. In this study the lifetime of the  $6_1^+$  of  $^{182}\text{W}$  (351 keV transition) was determined.

The Doppler shift of the emitted  $\gamma$  rays depends on their energy, the recoil velocity, and the angle of detection. Two-fold ( $\gamma$ - $\gamma$ ) events were sorted into three dimensional matrices for further analysis, based on the relative angle of each ROSPHERE detector ring. The Forward Ring (FF) refers to  $37^\circ$  detecting angle with respect to the beam axis and the Backward Ring (BB) refers to  $143^\circ$  angle. The obtained spectra for each distance are presented in Fig. 7 where the shifted (*s*) and the unshifted (*u*)

components of the  $6_1^+ \rightarrow 4_1^+$  g.s. band transition are shown to be separated in larger distances. The  $6_1^+$  state has a known lifetime of  $t_{1/2} = 8.2(9)$  ps [4], and can serve as a validation of the experimental method. The velocity of the  $^{182}\text{W}$  recoil nucleus after exiting the target is 0.833% c, or  $u = 2.49(18)$   $\mu\text{m}/\text{ps}$ .

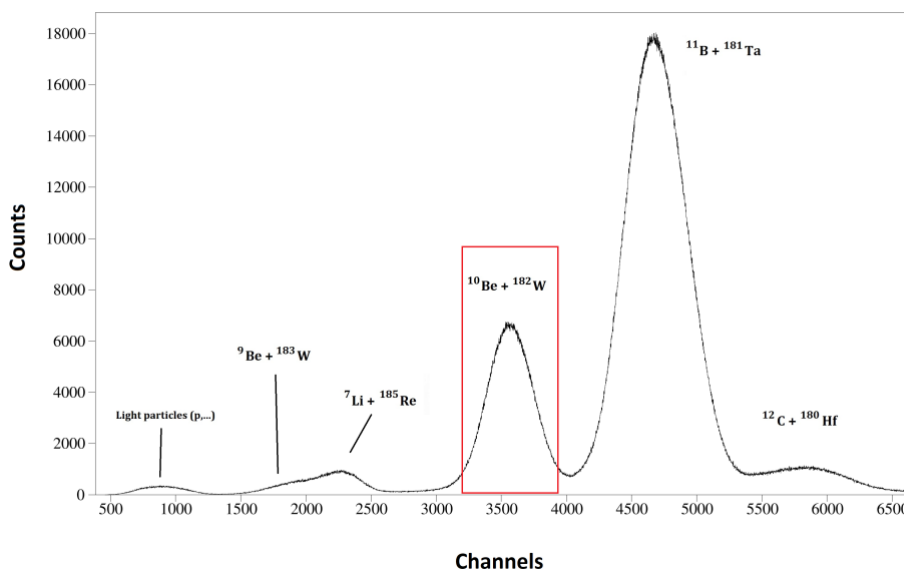


**Figure 5.** Typical particle spectrum recorded by the SORCERER detector array. Marked above each peak is the ejectile produced by the corresponding reaction channel.

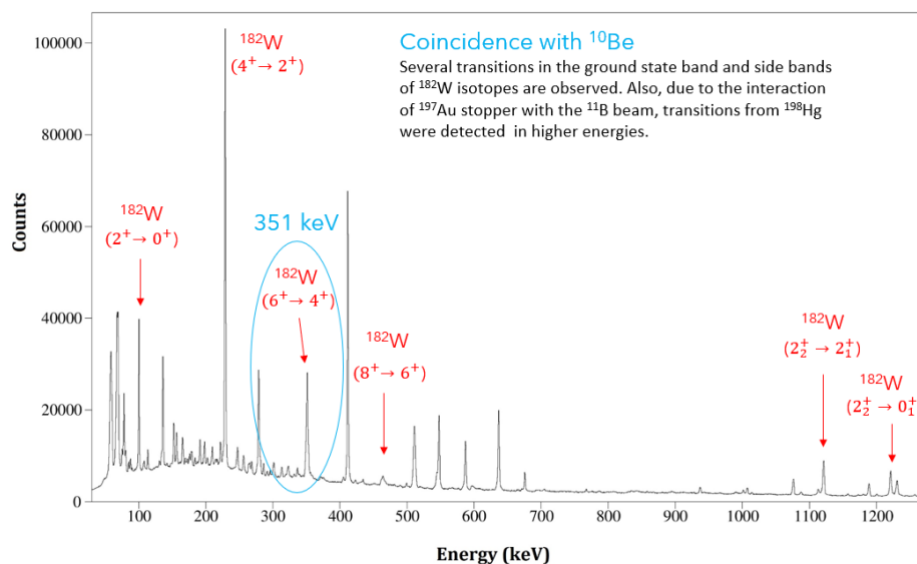


**Figure 6.** The  $\gamma$ - $\gamma$  symmetric spectra at 47 mev beam energy and 150  $\mu\text{m}$  distance

To address the issue of level feedings, it is preferable to work in coincidence mode and apply a gate on the Doppler-shifted ( $I^{SB}$ ) component of the 464 keV ( $8_1^+ \rightarrow 6_1^+$ )  $\gamma$  ray above the level of interest (see Fig. 4b). This gating method ensures that only the nuclei that are still in flight are selected for the analysis [7]. The basic relation for the determination of the mean lifetimes according to the DDCM in coincidence mode is given in Eq. (1).

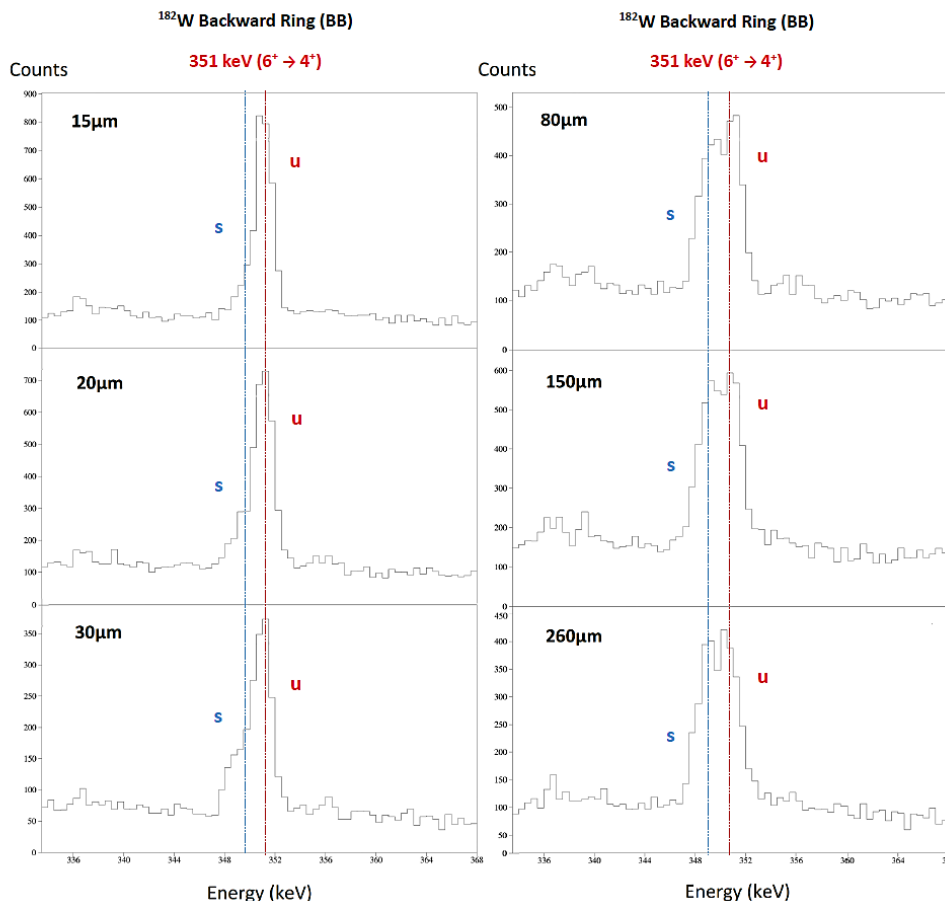


**Figure 7.** The shifted (*s*) and unshifted (*u*) components of the 351 keV  $\gamma$  ray of  $^{182}\text{W}$  are plotted for backward (BB) ring, for the six distances.

In Fig. 8, the intensities of the shifted  $I_{sA}^{SB}$  and unshifted  $I_{uA}^{SB}$  components of the A transition (351 keV) are plotted for each plunger distance. The experimental data points are described using a function consisting of second-order polynomials that are piecewise continuously differentiable. It is crucial to fit a smooth curve to the data points, especially in the sensitive region, typically found between 15-80  $\mu\text{m}$ . The quality of the curve description within this sensitive region is of utmost importance, while the description of points outside this range is less relevant. The fitted curve must exhibit specific characteristics, such as being monotonically increasing with exactly one inflection point located within the sensitive region. In Fig. 8, the unshifted component (blue  $\blacktriangle$ ) and shifted component (orange  $\blacksquare$ ) of transition A (351 keV) in coincidence with the shifted component of the feeding transition B (464 keV) are shown for the backward ring, which has higher statistics compared to the forward ring. Both unshifted and shifted intensities have been normalized using the counts of the strong  $4_1^+ \rightarrow 2_1^+$  transition (229 keV) for each target-to-stopper distance. The curve represents the fit of the normalized intensities of the shifted component  $I_{sA}^{SB}$  up to a target-to-stopper distance of 80  $\mu\text{m}$ .

In Fig. 9, the mean lifetime of the  $6_1^+$  state was determined to be  $\tau=10.35\pm 4.95$  ps, or equivalently, a half-life of  $t_{1/2}=7.18\pm 3.43$  ps. The plotted values of  $\tau$  against the distance are commonly referred to as the  $\tau$ -curve. This value is in agreement with the nominal value found in the literature, which is  $t_{1/2}=8.20\pm 0.90$  ps. The measured lifetime in Fig. 9 falls within the range of the literature value, despite the measured uncertainty of 4.95 ps is considerably larger than the literature uncertainty of 0.90 ps. The resulting lifetime is calculated as the weighted mean of individual  $\tau$  values, considering the intensity of

the unshifted component, the derivative of the intensity curve for the shifted component, and the recoil velocity within the sensitive region (15-80  $\mu\text{m}$ ) for the backward (BB) ring.

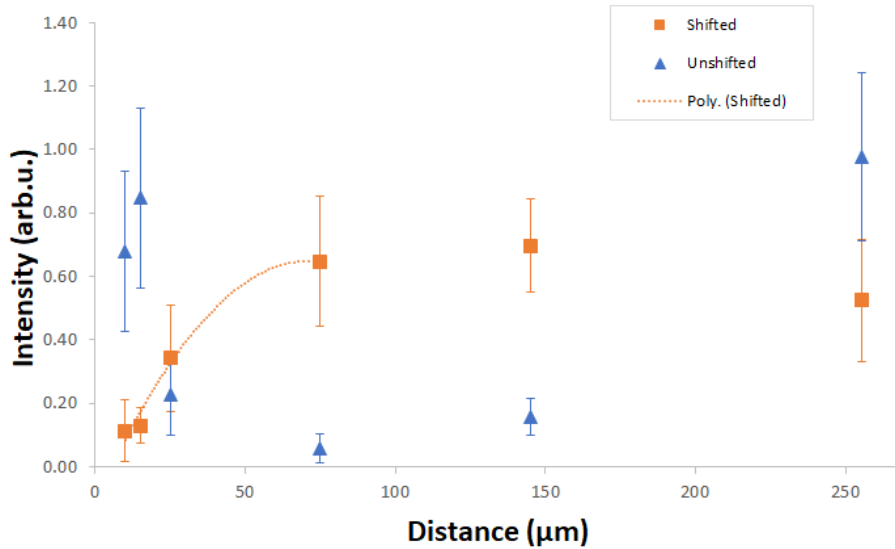


**Figure 8.** DDCM coincidence analysis of the  $6_1^+$  state in  $^{182}\text{W}$ . The dashed line is a fit with a second order polynomial to the shifted components in the sensitive region [7].

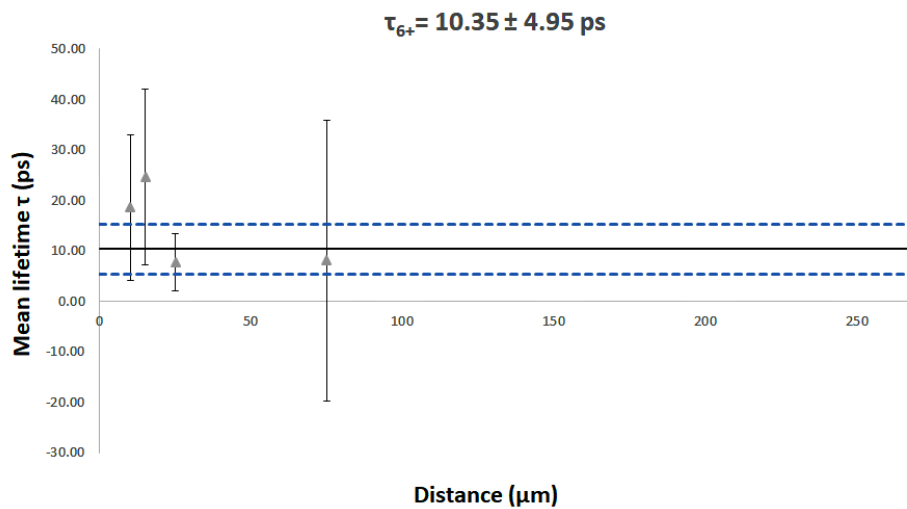


**Figure 9.** The  $\tau$ -curve calculated according to Eq. (1) in the sensitive region

The substantial uncertainties in the lifetimes predominantly influenced by statistical uncertainties in fitting the shifted and unshifted peaks. These uncertainties arise due to limited counts, particularly after employing the triple gating technique in HPGe detectors for ring-to-ring coincidences, and inherent statistical fluctuations. Correlations observed in measurements could arise from various sources like systematic errors, shared background contributions, or instrumental effects. Despite these challenges, the DDCM method has proven effective, yielding a measured lifetime of  $t_{1/2} = 7.18 \pm 3.43$  ps for the  $6_1^+$  state of  $^{182}\text{W}$ . This result is deemed acceptable, considering known lifetime values, the experimental setup, and available beam time.

## CONCLUSIONS

The results obtained from this experiment, particularly the validation of the lifetime for the  $6_1^+$  state of  $^{182}\text{W}$ , for the first time via the fusion evaporation reaction  $^{181}\text{Ta}(^{11}\text{B}, ^{10}\text{Be})^{182}\text{W}$  and the DDCM, underscore the efficacy of the Differential Decay Curve Method (DDCM) as an invaluable technique for such measurements. However, it is crucial to acknowledge various factors that can influence the precision of the obtained lifetime and broaden the applicability of this method to other states with comparable lifetimes. Nonetheless, the method appears effective in this instance, and a result for the lifetime  $t_{1/2}=7.18\pm 3.43$  ps is deemed acceptable for this nucleus, considering the known lifetime value from the literature and the experimental setup. Future endeavors involve refining experimental techniques, addressing inherent limitations, and formulating robust data analysis methods to enhance the accuracy and precision of lifetime measurements in nuclear physics research. These ongoing efforts, encompassing both techniques and challenges, contribute to the continuous advancement of our comprehension of nuclear structure and dynamics through precise lifetime measurements.

## Acknowledgments

This research work was supported by the Hellenic Foundation for Research and Innovation (HFRI) under the HFRI PhD Fellowship grant (Fellowship Number: 101742/2019) for AZ. The authors are thankful to the staff of the 9 MV Tandem Laboratory at Horia Hulubei National Institute of Physics and Nuclear Engineering for both their scientific and technical support during the experiment.



## References

- [1] R. Gupta et al., *Braz. J. Phys.* 52, 174 (2022); doi: 10.1007/s13538-022-01173-w
- [2] L. M. Robledo et al., *J. Phys. G* 6, 115104 (2009); doi: 10.1088/0954-3899/36/11/115104
- [3] K. Nomura et al., *Phys. Rev. C* 83, 054303 (2011); doi: 10.1103/PhysRevC.83.054303
- [4] NNDC. National Nuclear Data Center, <http://www.nndc.bnl.gov/>
- [5] D. Bucurescu et al., *NIM A* 837, 1 (2016); doi: 10.1016/j.nima.2016.08.052
- [6] T. Beck et al., *NIM A* 951, 163090 (2020); doi: 10.1016/j.nima.2019.163090
- [7] A. Dewald et al., *Prog. Part. Nucl. Phys.* 67, 786 (2012); doi: 10.1016/j.ppnp.2012.03.003
- [8] P. Vasileiou et al., *HNPS Adv. Nucl. Phys.* 28, 112 (2022); doi: 10.12681/hnps.3612
- [9] P. J. Nolan and J. F. Sharpey-Schafer, *Rep. Prog. Phys.* 42, 1 (1979); doi: 10.1088/0034-4885/42/1/001
- [10] P. Petkov, *NIM A* 349, 289 (1994); doi: 10.1016/0168-9002(94)90636-X
- [11] G. Böhm et al., *NIM A* 329, 248 (1993); doi: 10.1016/0168-9002(93)90944
- [12] A. Dewald et al., *Nucl. Phys. A* 545, 822 (1992); doi: 10.1016/0375-9474(92)90531-N